JGR Earth Surface

RESEARCH ARTICLE
10.1029/2020JF006058

Evaluating the Relationship Between Meander-Bend Curvature, Sediment Supply, and Migration Rates

Mitchell Donovan[1], **Patrick Belmont**[1], **and Zoltán Sylvester**[2]

[1]Department of Watershed Sciences, Utah State University, Logan, UT, USA, [2]The University of Texas at Austin, Bureau of Economic Geology, Austin, TX, USA

Key Points:

- Migration rates are negligible and migration-curvature relations break down along reaches with low sediment supply
- Curvature-migration relationships consistently peak at lag distances of ~2.5 ± 0.25 channel-widths regardless of climate and geology
- Results support empirical, flume, and theoretical findings of a direct monotonic relation between channel curvature and migration rates

Correspondence to:
M. Donovan,
mdonovan@aggiemail.usu.edu

Citation:
Donovan, M., Belmont, P., & Sylvester, Z. (2021). Evaluating the relationship between meander-bend curvature, sediment supply, and migration rates. *Journal of Geophysical Research: Earth Surface*, *126*, e2020JF006058. https://doi.org/10.1029/2020JF006058

Received 12 JAN 2021
Accepted 17 FEB 2021

Abstract River meander migration plays a key role in the unsteady "conveyor belt" of sediment redistribution from source to sink areas. The ubiquity of river meandering is evident from remotely sensed imagery, which has allowed for long-term, high-resolution studies of river channel change and form-process relationships. Empirical, experimental, and theoretical research approaches have described two distinct relationships between channel curvature and river channel migration rates. In this study, we employ a novel application of time-series algorithms to calculate migration rates and channel curvature at sub-meander bend length scales using 6 decades of aerial imagery spanning 205 km of the Minnesota River and Root River, Minnesota, USA. Results from the Minnesota River provide the first empirical evidence demonstrating how migration-curvature relations break down for rivers with low sediment supply, which is supported by the Root River data set. This not only highlights the importance of sediment supply as a driver of river migration, but also supports a simple means to detect river reaches lacking sediment supply. Furthermore, results from both rivers demonstrate that sub-meander bend measurement scales are most appropriate for studying channel migration rates and further indicate that a quasi-linear relationship—rather than the more commonly inferred peaked relationship—exists between channel curvature and migration rates. The highest migration rates are associated with the highest measured channel curvatures in our data set, after accounting for a spatial lag of $2.5 \pm^{0.3}_{0.2}$ channel widths. These findings are consistent with flume experiments and empirical data across diverse geologic and climatic environments.

Plain Language Summary River meander migration plays a key role in the redistribution of sediment from uplands and headwaters to valley bottoms, lakes, reservoirs and the ocean. In this study, we measure both river migration rates and curvature at high resolution (every 10-m) using six-decades of aerial imagery spanning 205 river-km of the Minnesota and Root rivers, Minnesota, USA. Our results demonstrate how differences in measurement scales led to different interpretations in previous research, and that high-resolution measurements are most useful for understanding curvature-migration relationships. The highest migration rates are associated with the highest measured channel curvatures, after accounting for a spatial lag of 2.5 ± 0.25 channel widths. These findings are consistent with flume experiments and empirical data across diverse geologic and climatic environments. Lastly, we demonstrate that curvature-migration relations cease for rivers with low sediment supply. This finding highlights the importance of sediment supply as a driver of river migration and establishes a simple means of detecting river reaches lacking bedload sediment transport.

1. Introduction

1.1. Background—River Meander Migration and Curvature

River meander migration is one of the most ubiquitous processes shaping and redistributing mass on Earth's surface. The forms and patterns of river meander development have fascinated scientists since the early 20th century (Brice, 1974; Davis, 1902; Leopold & Wolman, 1960; Schumm, 1965; Wolman & Leopold, 1957), capturing even Albert Einstein, who provided insight on why meander wavelength scales with channel width (Einstein, 1926). The complexity inherent to meander migration is reflected in studies spanning multiple orders of spatial and temporal magnitude, from individual meander bends (Dietrich et al., 1979; Kasvi et al., 2017), to geologic-scale evolution of floodplains and valleys (Gran et al., 2013; Howard, 1996; Sun et al., 1996). Such studies improve models predicting where and when migration will occur,

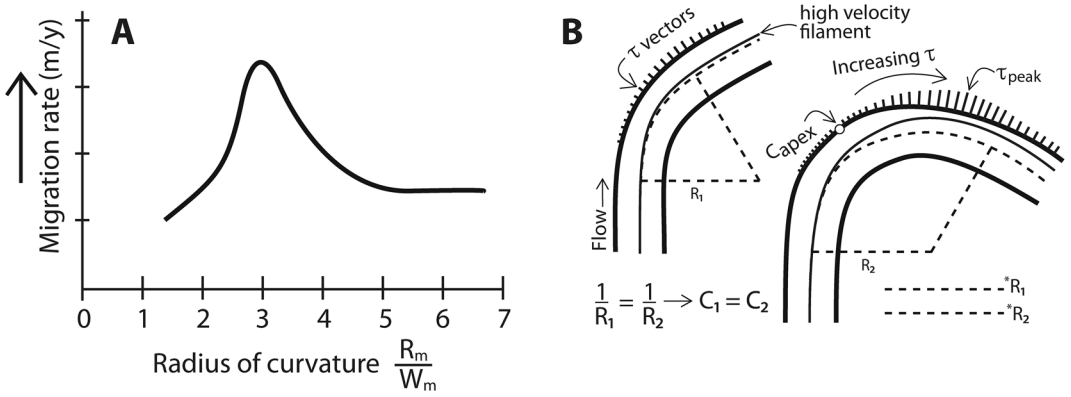

Figure 1. Competing ideas regarding the relation between curvature and meander-bend migration. (a) Meander-bend averaged migration plotted as a function of meander-bend averaged radius of curvature normalized by channel width (R/W), as reproduced from Hickin and Nanson (1975). The x-axis is the bend-averaged radius of curvature normalized by channel width, which is inversely related to curvature (see Equation 2). (b) Conceptual diagram, adapted from Furbish (1988), illustrating how two meander bends can have the same bend-averaged radius of curvature despite distinct differences in shear stress along the outer bank. Thus, despite having the same radius of curvature, R_2 will migrate faster due to higher shear stresses. $*R_1$ and $*R_2$ were transposed from each of the curves as evidence that the radii are equal.

providing useful information for environmental management, protection of infrastructure, and stream restoration. Remotely sensed imagery is commonly used to measure changes in river planform in response to changes in land use, urbanization, deforestation, and dam building or removal (Constantine et al., 2014; Donovan et al., 2015, 2016; Gurnell et al., 1994; Gaeuman et al., 2005; Hickin & Nanson, 1984; Lauer & Parker, 2008; Morais et al., 2016).

Using a combination of aerial imagery and U.S. Geological Survey (USGS) topographic maps, Brice (1974) established seven generalized classes of meander development based on predictable and persistent patterns over broad scales, all of which reflect localized feedbacks between sediment loads and the flow of water (Constantine et al., 2014). Contrasting gradients in stresses, which increase along the outer bend and decrease along the inner bend, drive differential erosion and deposition of sediment (Bagnold, 1960; Dietrich et al., 1979; Leopold & Wolman, 1960). Centrifugal forces and shear stresses along the outer bank of a meander bend increase with curvature of the bend, and thus, migration rates should vary directly with curvature (Furbish, 1988; Howard & Knutson, 1984). This relation has been shown to decrease again in very high curvature bends, where a variety of separation zones can develop and shear stresses on the outer bank can be reduced (e.g., Blanckaert, 2011). Curvature (C) is the degree to which a segment/surface deviates from a line/plane and is the reciprocal of the radius of curvature (R). Although the outer bank shear stress increases with bend curvature, some empirical measurements indicate that migration rates peak at a radius of curvature that is 2–3 times the channel width (R/W ~2–3) when measurements are averaged over the scale of a meander bend (Figure 1a; Hickin & Nanson, 1975, 1984). This relationship has been observed in many subsequent studies (e.g., Finotello et al., 2018; Güneralp & Rhoads, 2008; Hooke, 2003; Hudson & Kesel, 2000; Nicoll & Hickin, 2010).

Bends with the same average curvature can have different degrees of asymmetry, suggesting that a single value of bend-averaged curvature may be associated with multiple patterns of shear stress (Furbish, 1988). For example, the two bends in Figure 1b have the same bend-averaged curvature but exhibit large differences in flow asymmetry and shear stress due to differing bend lengths. The longer bend has larger shear stresses along the outer bank, and therefore will have faster migration rates compared to the shorter bend. Migration trajectories along a bend depend not only on local curvature, but also on cumulative upstream curvature (Furbish, 1988; Howard & Knutson, 1984), which varies with bend length. Thus, a highly resolved (sub-meander scale) approach that accounts for non-local (upstream and potentially downstream) effects is required to fully understand the relationship between curvature and meander migration rates. While the results and empirical relationship established in Hickin and Nanson (1975) reflect rigorous science and a

breakthrough in understanding curvature-migration rate dynamics, a significant fraction of subsequent research largely overlooked the concerns outlined in Furbish (1988), summarized in Figure 1.

Models relating bank erosion to local curvature reproduce the peaked relation between local migration and curvature (Begin, 1981). However, others note that using local curvature to model meander development results in bend form growth lacking the asymmetry (Carson & Lapointe, 1983) and spatial heterogeneity that is observed in the complex planform adjustments (Güneralp & Rhoads, 2011) common to many meandering rivers. Howard and Knutson (1984) showed that meander migration models using both local curvature and upstream curvature, weighted as a function of distance upstream, are better able to simulate asymmetrical bend development, downstream translation, and cutoffs typical of natural meandering streams.

Measuring migration and curvature at a high resolution enables the analysis of sub-meander scale flow dynamics that drive heterogeneity in meander migration throughout a bend. A high-velocity flow filament is directed toward the outer bank, reaching the outer bank downstream of the bend apex (Dietrich et al., 1979; Kasvi et al., 2017; Seminara, 2006), and not always within the meander bend (Leopold & Wolman, 1960). Shear stress and erosion increase downstream from the bend apex along the outer bank where the highest velocities persist due to centrifugal force and acceleration of secondary flow currents (Dietrich et al., 1979; Seminara, 2006; Zhou et al., 1993). Meanwhile, the inner bank is associated with lower flow velocities, and when combined with adequate sediment supply, may experience deposition and point bar growth (Carson & Lapointe, 1983). As point bars grow along the inner bank, they increasingly push high-velocity flow paths toward the outer bank, thus increasing shear stress and erosion along the outer bank. This mechanism linking sediment supply and point bar development to erosion along the outer bank is commonly referred to as "bar push" (Dietrich & Smith, 1983; Eke et al., 2014). Alternatively, a "bank pull" process occurs when bars grow in response to erosion of an outer bank. The spatial lag between bend apices and peak migration rates ultimately reflects the inertial properties of the fluid as well as a lag in shear stress associated with secondary flow development, and thus, peak migration should be downstream of the bend apex. Exceptions to this may exist in rare laboratory or field settings where extreme curvatures may exhibit a "protective" effect on downstream channel banks, often as a result of geologic or anthropogenic influences. The downstream lag distance between the peak in curvature and the peak in outer bank shear stress or migration rate may be influenced by other variables such as meander arc length, width:depth ratios, friction or flow resistance, flow depth, inner-bank bar angle, size of the point bar, and suspended sediment concentration (Furbish, 1991; Güneralp & Marston, 2012; Güneralp & Rhoads, 2009; Patnaik et al., 2014; Seminara, 2006; Zhou et al., 1993).

By measuring migration rates and channel curvature at sub-meander bend scales, Sylvester, Durkin, and Covault (2019) provided empirical evidence to support a direct relationship between channel curvature and downstream migration rates for seven Amazonian rivers with high sediment supply and transport. When associating spatially lagged values, migration rates continually increased as curvature increased. Deviations from the general trend were attributed to reduced bank erodibility. The authors concluded that peaked curvature-migration relationships (e.g., Hickin & Nanson, 1975) result from associating bend-averaged values of curvature and migration rate, without considering within-bend variability and the spatial lag between the two.

Channel migration not only reflects local patterns of shear stress, but also feedbacks between sediment loads and the flow of water (Constantine et al., 2014; Neill, 1971, 1984). When sediment supply exceeds the transport capacity of a channel, deposition leads to steeper channel slope, adjustments in channel patterns, and point bar growth (Ashworth, 1996; Engel & Rhoads, 2012; Kelly, 2019; Venditti et al., 2012). As channel bars grow, so do the positive feedbacks associated with the asymmetry in the channel bed, flow velocities and depths, and shear stresses increase the probability of lateral migration via bar push (Eke et al., 2014). To date, we find no evidence supporting whether channels lacking adequate sediment supply exhibit reductions in asymmetric flows and shear stresses sufficient to dampen or halt bar growth and thus, channel migration. Rivers within the Amazon River Basin exhibit some of the highest sediment transport rates in the world, and exhibit migration rates that are consistently linked to high sediment supply and bar push feedbacks (Constantine et al., 2014). It remains to be seen if the direct relationship between curvature and migration (Sylvester, Durkin, & Covault, 2019) can be replicated in other settings, and whether such relationships hold in the absence of extremely high sediment transport rates such as those in the Amazon

River Basin (Martinelli et al., 1989; Milliman & Meade, 1983). To address this knowledge gap, we evaluate the relationship between channel curvature and migration in a completely different climatic and geological setting. Further, we use the Minnesota River to evaluate curvature-migration rates along a well-constrained, pronounced gradient in bedload sediment transport, ranging from bedload supply that greatly exceeds capacity to essentially zero bedload supply. Specifically, we address the question: how does sediment supply, relative to transport capacity, affect river channel migration rates and the curvature-migration relationship?

We evaluate the relationship between channel curvature, migration rates, and bar geometry in the Minnesota River and Root River, Minnesota, USA, using repeated aerial images spanning large temporal (eight and six sets of air photos over 76 years) and spatial scales (205 river km). We use bathymetric and sediment-transport data to explore linkages between sediment supply, curvature, and migration rates for the 180-km reach of the Minnesota River (Groten et al., 2016; Kelly, 2019). Data from the Root River are used as a second case to evaluate the persistence of curvature-migration trends where sediment supply appears to be consistently high in the downstream direction, due to floodplain remobilization (Donovan & Belmont, 2019; Vaughan et al., 2017). We first evaluate the relationship between meander-bend averaged curvature and migration and compare these results to analyses of spatially lagged values of curvature and migration rates measured at sub-meander scales to understand whether measurement length scale influences the form of the relationship between channel curvature and migration rates (i.e., migration rates increase as a continuous function of curvature, or peak at intermediate curvature values). Specifically, we address the questions: What is the magnitude and variability in the spatial lag between curvature and migration rate when measured at sub-meander bend scales? Are migration rates, the lag distance between curvature and migration, and the strength of the curvature-migration relationship sensitive to sediment supply?

2. Study Area and Data

We evaluate curvature-migration relationships using channel change along centerlines derived from aerial photographs spanning approximately 180 km of the Minnesota River between the towns of Mankato and Fort Snelling, near the confluence with the Mississippi River. Six sets of images (1937, 1951, 1964, 1980, 1991, and 2013) were available along this portion of the river, which has been the focus of multiple recent geomorphic studies due to its unique geomorphic history and longitudinally contrasting sediment dynamics (Call et al., 2017; Lauer et al., 2017; Lenhart et al., 2013; Libby, 2017; Kelly & Belmont, 2018). About 13,400 years ago, the outpouring of glacial Lake Agassiz caused 70 m of incision of the mainstem Minnesota River Valley (Clayton & Moran, 1982; Lepper et al., 2007; Matsch, 1983; Shay, 1967), which has resulted in multiple knickpoints and exposure of highly erodible glacial sediments along tributary valleys (Belmont, 2011; Gran et al., 2013; Jennings, 2010). In addition, the river has been responding to contemporary land use and precipitation changes over the last 80 years, which have increased flows by 50%–250% (Belmont, Dogwiler, & Kumarasamy, 2016; Kelly et al., 2017; Foufoula-Georgiou et al., 2015; Novotny & Stefan, 2007; Schottler et al., 2014). Recent increases in flow from artificial drainage have amplified rates of lateral channel migration (Belmont et al., 2011; Libby, 2017) and increased channel widths by 52% since 1938 (Lauer et al., 2017; Schottler et al., 2014).

Within the 180-km study reach, the channel exhibits abrupt reductions in sediment grain size and slope, and changes in channel-bar geometry, roughly 100-km downstream near the town of Belle Plaine (Groten et al., 2016; Kelly, 2019; Figure 2). Between 2011 and 2014, the USGS monitored suspended sediment concentrations (SSC), bedload transport, and particle sizes at five locations, alongside continuous Acoustic Doppler velocity measurements to support acoustic surrogate SSC modeling (Groten et al., 2016). SSC and bedload samples were obtained concurrently in wadable and non-wadable conditions at 20 evenly spaced increments within each cross section. Mean and median of measured loads showed significant reductions from the upstream reach (250–341 tons/day, blue reach in Figure 2) to the downstream reach (3–69 tons/day, red reach in Figure 2). Three methods were then used to estimate total annual sediment yield, load and bedload for each site, with consistent results (i.e., not significantly different) showing demonstrable reductions in the magnitude of total annual bedload downstream of Belle Plaine (red reach, Figure 2). Particle-size analyses revealed that median bedload particle size dropped from 1 to 0.34 mm at downstream sampling locations, which is consistent with bed and point bar samples collected between 2013 and 2016 (Kelly, 2019). Kelly (2019) surveyed 234 km of the Minnesota River bathymetry at high flow each year

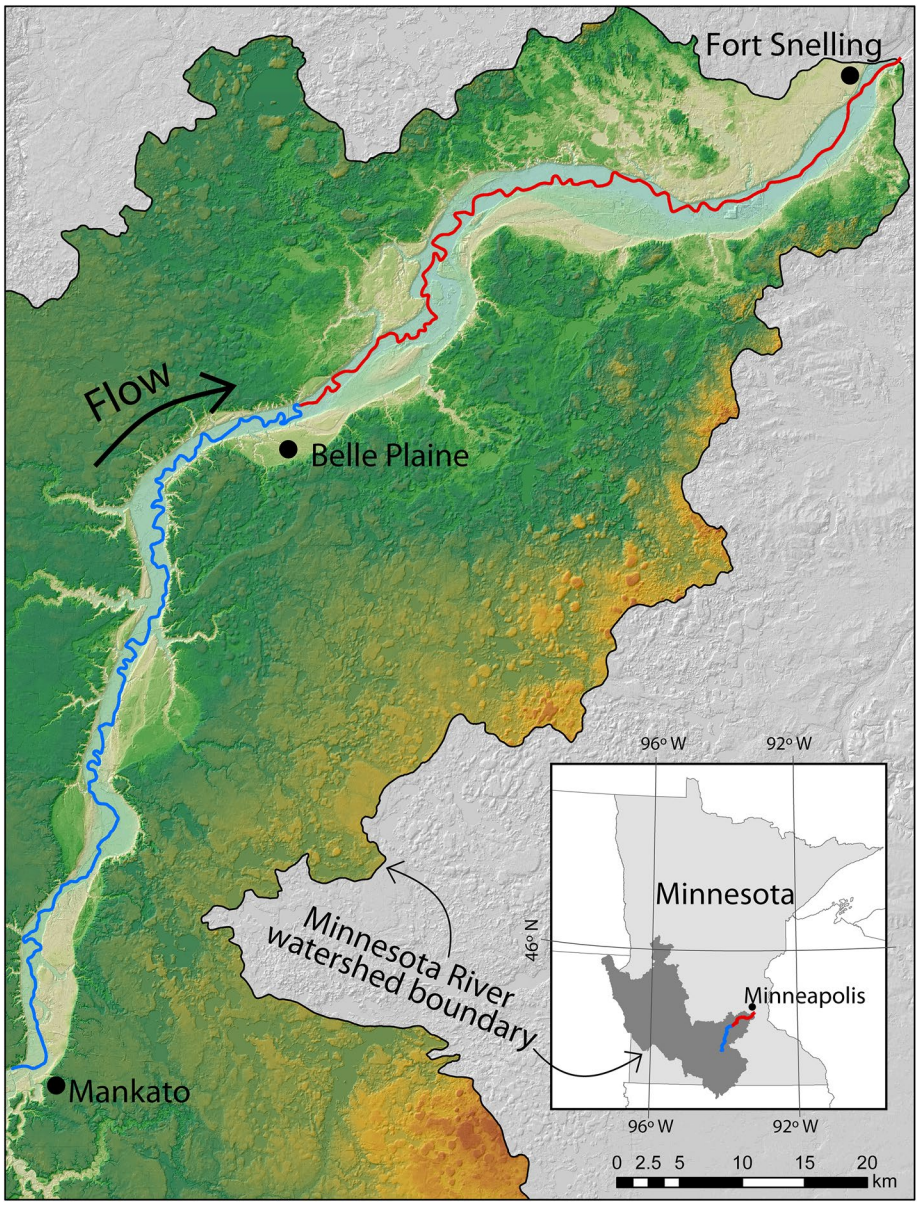

Figure 2. Location map of the study reach along the Minnesota River, which spans from the town of Mankato to Fort Snelling (center). Unique upstream and downstream reaches are highlighted in blue and red, respectively. The bed and bars of the downstream reach (red) of Belle Plaine contains fine sands, silts, and clays, compared to the upstream reach (blue), which consists of coarse sands and gravels. Further, the river gradient abruptly reduces by 75% near the town of Belle Plain (Groten et al., 2016).

between 2013 and 2016 using an Acoustic Doppler Current Profiler, resampled to 1-m^2 grids. The bathymetric surveys were combined with bar geometry (width and height) field measurements, which revealed large, wide channel bars along the upstream reach contrasted by tall, narrow point bars composed of finer grained sediment in the downstream reach. These differences in bar forms lead to distinct hydraulic regimes. Specifically, the large, wide bars in the upper reach cause accentuated lateral flow paths and helical flow patterns, thus generating bar-push feedbacks (Dietrich et al., 1983). In contrast, the tall, fine-grained, narrow bars found in the lower reach grow only in response to a "bank-pull" process and do not grow wide enough to influence cross-channel secondary flow structures (Kelly, 2019). The excellent constraints on sediment supply, channel morphology and hydraulics along the Minnesota River provide a rare opportunity to study the role of sediment supply in the relationship between channel curvature and meander migration rates.

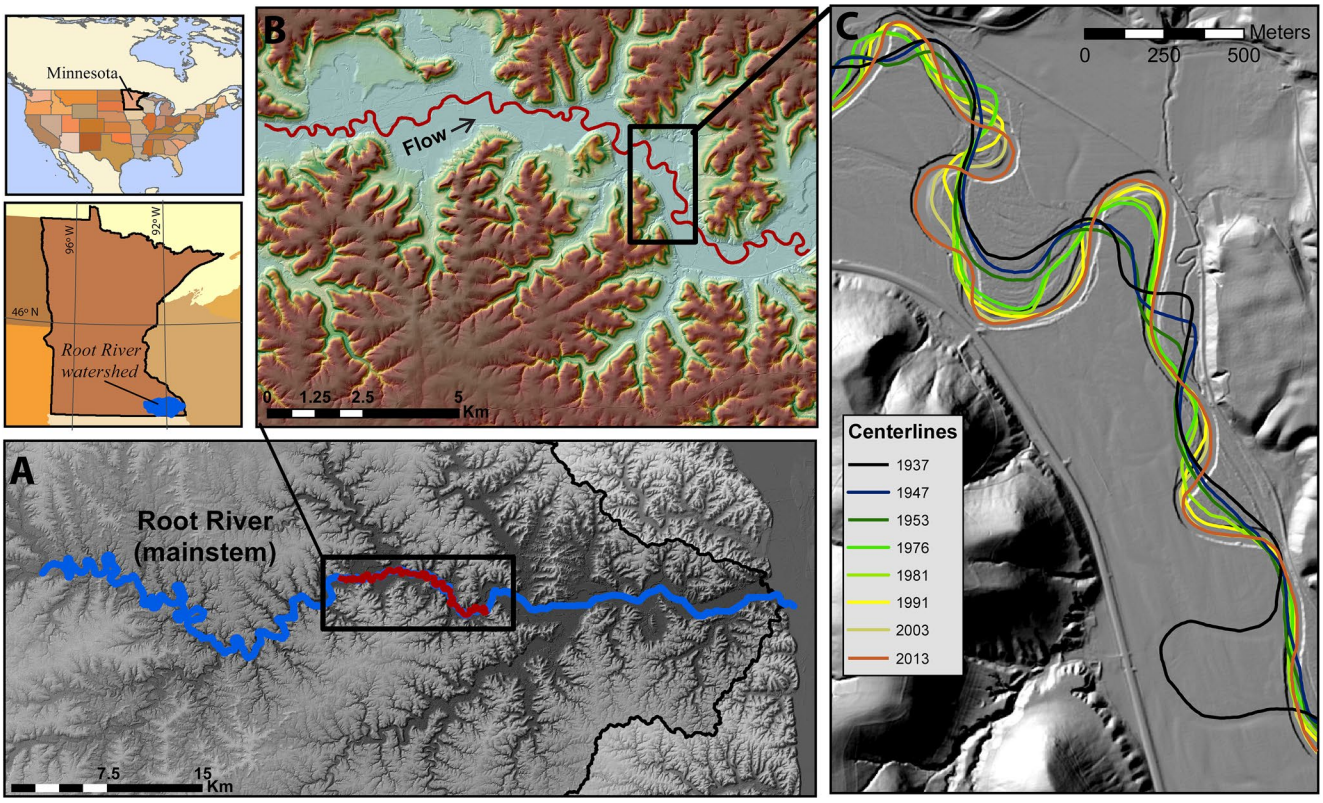

Figure 3. Overview of Root River within the North American continent and state of Minnesota (top left). (a) The mainstem drains from left to right into the Mississippi River. (b) The 25-km segment of the Root River chosen for analysis. (c) An example of centerlines derived from delineations for each of the eight sets of images spanning 1937–2013. The underlying shaded relief image was derived from 3-m lidar elevation data (Minnesota Department of Natural Resources and Minnesota Geospatial Information Office, 2012).

We extend our analysis to include approximately 25 km of the Root River, Minnesota, a single-threaded, meandering sand- and gravel-bedded river that drains into the Mississippi River (Figure 3a). The 25-km reach (Figure 3b) chosen for analysis contains the most active meander bends of the mainstem river, which has been studied extensively (Belmont, Dogwiler, & Kumarasamy, 2016; Belmont, Dogwiler, Czuba et al., 2016; Stout & Belmont, 2013; Stout et al., 2014; Souffront, 2014). Meander bends in this reach are intermittently laterally confined by either natural or anthropogenic impingements (Figure 3c). Channel confinement and variable riparian conditions provide sufficient irregularity in erodibility to test whether a simple curvature-migration model remains robust despite variable conditions. We used eight sets of images (1937, 1947, 1953, 1976, 1981, 1991, 2003, and 2013) with sufficiently similar time intervals to the Minnesota River analyses that encompass significant channel adjustment (Donovan & Belmont, 2019). While no sediment-transport data exist for the Root River, previous research has demonstrated the importance of migration and widening as an active and dominant source of sediment for the Root River (Belmont, Dogwiler, & Kumarasamy, 2016; Belmont, Dogwiler, Czuba et al., 2016; Stout et al., 2014). Further, the Root River has some of the steepest relationships between Q and TSS (discharge-total suspended sediment) in the state of Minnesota based on over 10 years of sampling since 2000 (Vaughan et al., 2017). TSS and suspended sediment concentration (SSC) both measure solids throughout the water column sampled and are generally correlated, but TSS measurements are a subsample of particles used in SSC protocols. The steepness of the Q-TSS relationship for the Root River is due largely to the predominance of near-channel sediment sources (Vaughan et al., 2017) and to the fact that approximately half of bank sediments are comprised of sand (Souffront, 2014). Thus, there is significant evidence that sediment supply is relatively high in the Root River, similar to the upstream reach of the Minnesota River (blue reach, Figure 2). If sediment supply and transport conditions are critical for modulating the relationship between channel curvature and meander migration rates, we hypothesize that the Root River relationships will emulate those of the upstream reach

of the Minnesota River, and will be markedly different from the observations made in the downstream reach of the Minnesota River.

3. Methods

3.1. Measuring Curvature and Channel Planform

For each year of imagery, channel banks were delineated as described in Donovan et al. (2019). Briefly, bank lines were interpolated to channel centerlines and converted to coordinate points in 10-m increments. At each increment, channel width was calculated using the Planform Statistics Toolbox. For each sequential pair of images ($n = 7$ for Root River, $n = 5$ for the Minnesota River), bank migration was measured at each 10-m increment along the channel using a dynamic time warping algorithm (DTW).

DTW was originally developed to correlate time series (e.g., Lisiecki & Lisiecki, 2002) and has been shown to greatly reduce computation time while improving bank-migration trajectories compared to typical nearest neighbor algorithms (Sylvester, Durkin, & Covault, 2019). DTW uses a cost matrix to minimize the sum of distances between signals, rather than minimizing the individual distance. DTW avoids bunching and/or large gaps between nodes on the terminal end of trajectories by minimizing the sum of trajectories, rather than individual trajectories. Thus, as the distance between two centerlines increases, the performance of DTW computations improves relative to nearest neighbor algorithms. The DTW implementation we have adapted for use in our migration rate calculations is available at https://github.com/dpwe/dp_python (Ellis, 2014). For further details on methods of calculating migration and associated uncertainty, see Donovan et al., (2019).

Subsequent to DTW computations, we manually identified and filtered out measurements within meander bend cutoffs before performing subsequent analyses. Curvature (units, m^{-1}) was calculated using the x and y components of each point's Cartesian coordinates:

$$C = \frac{x'y'' - y'x''}{\left(x'^2 + y'^2\right)^{3/2}}, \tag{1}$$

where x′ and x″ are the first- and second-order derivatives of the x coordinate. Curvature is the reciprocal of the radius of curvature, R (Equation 2):

$$C = \frac{1}{R}; \therefore \frac{R}{W} = \frac{1}{C \cdot W}, \tag{2}$$

and thus, is inversely related to width-normalized radius of curvature (R/W) that is commonly plotted against migration rates (e.g., Hickin & Nanson, 1975). Curvature and migration rates were smoothed using a Savitzky-Golay filter to reduce noise (Motta et al., 2012; Sylvester, Durkin, & Covault, 2019). Savitzky-Golay filtering retains local precision without distorting the signal by fitting low-degree polynomials to successive subsets of data points (Savitzky & Golay, 1964). The code used to estimate curvature and migration rates is available at https://github.com/zsylvester/curvaturepy (see also Sylvester, Durkin, & Covault, 2019).

3.2. Discerning Spatial Relationships in Migration and Curvature

After generating longitudinal profiles of migration and curvature, we employed a signal processing algorithm (scipy.signal.find_peaks) in Python to find local maxima and minima (both are referred to as "peaks"). An individual point would be defined as a peak if it was greater than adjacent (upstream or downstream) values within 40 m (Figure 4). By using simple/minimal criteria to detect peaks, we eliminated false negatives and then manually removed false positives, retaining only curvature peaks that could be paired with peaks in migration rates. The lag distance between paired peaks in migration rates and curvature was the distance between each set of peaks, as measured along the channel centerline. Lag distances were normalized by the mean of channel widths between the peaks:

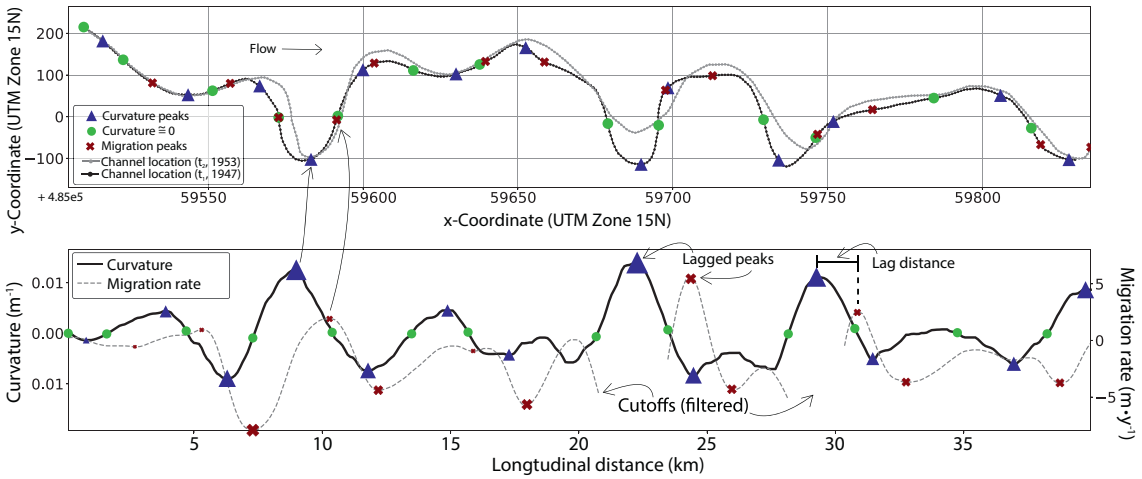

Figure 4. An example of curvature and migration rate profiles plotted alongside their local maxima and minima (blue triangles = curvature peaks, red Xs = migration peaks). (Top) Planform view. (Bottom) Longitudinal/graphical view. Locations of zero curvature are plotted as green points. Lag distances between peaks were calculated as the longitudinal difference, divided by the local average river width. Channel cutoffs were manually filtered and discarded prior to the analyses.

$$L^* = \frac{\mathrm{Loc}_{\mathrm{Cpk}} - \mathrm{Loc}_{\mathrm{Mpk}}}{\dot{W}_{\mathrm{Cpk:Mpk}}}, \tag{3}$$

where L^* is the dimensionless lag, $\mathrm{Loc}_{\mathrm{Cpk}}$ is the location of peak curvature, $\mathrm{Loc}_{\mathrm{Mpk}}$ is the location of peak migration rate, and $\dot{W}$ is the ensemble mean channel width between the two peaks.

We evaluated the magnitude and variability of these lags using summary statistics and histograms. We have also computed the derivatives of curvature and migration and identified paired zero crossings in curvature and migration. Zero crossings provided an additional method to evaluate spatial lags. As before, the distances between paired zero crossings were normalized to average channel width between the paired inflections, thereby providing an independent test to evaluate the consistency in magnitude and variability of spatial lags.

Each peak in meander migration occurred downstream of a point at which curvature was zero, representing the initiation of the current meander bend and development of asymmetrical flow that increases shear stress along the outer bank (Furbish, 1988). While flow is not necessarily symmetrical at the location of zero curvature, it is a reasonable approximation of where the high-flow velocity path transitions from one bank to the other.

We manually categorized bank erodibility at each 10-m increment along the Root River as "constricted", "resistant", or "freely meandering" (2, 1, and 0, respectively) based on the outer, resisting bank. Segments classified as "constricted" were confined by a valley constriction, colluvium, or anthropogenically constructed embankment/structure (e.g., bridge crossing) along the outer bank. "Resistant" reaches were bounded by tree or shrub vegetation dense enough to mask the underlying ground or streambanks, and were presumed to be less erodible than "freely meandering" reaches that lacked extensive root systems (Abernethy & Rutherfurd, 2000; Micheli & Kirchner, 2002; Peixoto et al., 2009). Based on ranked values of resistance, we tested whether reaches with higher cumulative resistance had greater lag distances.

We cross-correlated a series of moving windows containing a subset of the curvature and migration profiles (using the scipy function "scipy.signal.correlate") to evaluate the spatially lagged relationship between migration and curvature signals, rather than analyzing only individual points (i.e., peaks and inflections). For each window, the two series were continually displaced relative to one another and cross-correlated at each degree of displacement. The displacement with highest signal cross-correlation was interpreted as the optimal lag distance between curvature and migration rate signals. The lag distance (meters) was normalized to

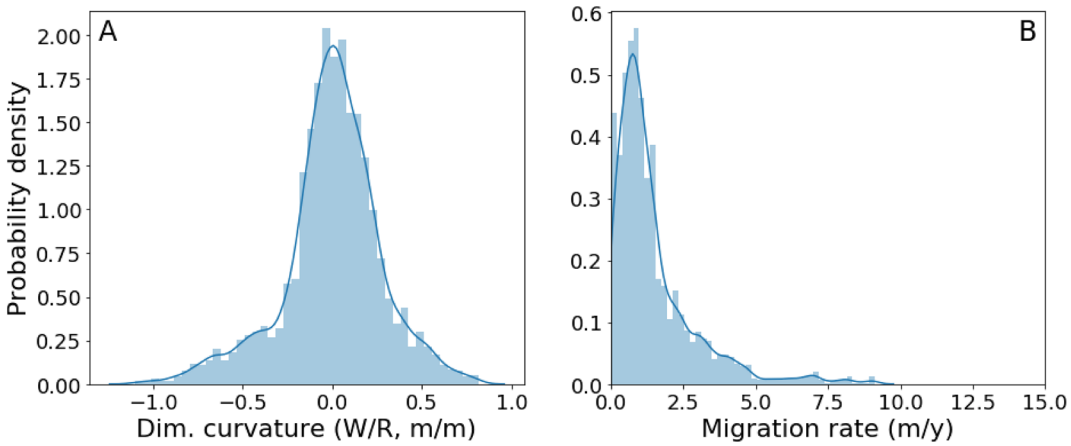

Figure 5. (left) Distribution of dimensionless curvature along the Root River, derived from imagery obtained in 1981. (right) Distribution of Root River migration rates measured between 1981 and 1991.

the mean channel width within the moving window. We tested window sizes spanning 2–20 channel widths (100–2,000 m) to encompass distances within a geomorphically plausible range.

3.3. Distinguishing the Form of Curvature-Migration Relationships

Prior literature has debated whether curvature-migration relationships are monotonic (i.e., migration continuously increases with increasing curvature), or peaked (i.e., exhibiting a maximum at low to moderate curvature values; R/W of 2–3, or W/R ~0.3–0.4; Figure 1a). In order to frame results in the context of previous studies, we first plot bend-averaged values of R/W and migration (e.g., Hickin & Nanson, 1975; Hooke, 2003; Hudson & Kesel, 2000; Nanson & Hickin 1983; Nicoll & Hickin, 2010). Subsequently, we directly evaluate the relationship between local migration and dimensionless curvature values (W/R) to consider the sub-meander bend relationship. We account for the phase lags in curvature and migration signals by plotting lagged local values (peaks and inflections) of curvature and migration. In doing so we can (1) more clearly evaluate the relationship between curvature and migration, rather than the bend-averaged radius of curvature (R) and (2) account for spatial lags between curvature and migration (Furbish; 1991, 1988; Sylvester, Durkin, & Covault, 2019). If plots from both approaches show a peak in migration at R/W ~2–3 (equivalent to 0.3–0.4 W/R), the implication is that neither measurement scale nor accounting for spatial lags alter the peaked relationship found by Hickin and Nanson (1975). Conversely, if plotting the local-scale lagged values of curvature and migration illustrates a monotonic, direct trend, while the bend-averaged approach exhibits a peaked envelope curve, we can conclude that there is empirical support for the idea that spatial measurement scale directly influences interpretations regarding the form of the curvature-migration relationship (Furbish, 1988; Howard & Knutson, 1984; Sylvester, Durkin, & Covault, 2019).

4. Results

4.1. Curvature and River Width Summary Statistics

For both the Minnesota and Root rivers, dimensionless curvature values are normally distributed around zero, with a total range of approximately −1 to 1 (Figure 5a). Migration rates follow a long-tailed, right-skewed distribution (i.e., many small rates and decreasing numbers of higher rates) with median values on the order of 0.5–1.5 m/year and maximum rates reaching approximately 15 m/y for both rivers (Figure 5b). The mean width of the Minnesota River increased from 70 to 102 meters throughout the period of study (1937–2013). For the 25-km Root River study reach, mean channel width varies from 47 to 55 m from decade to decade.

Our final data set, after removing cutoffs and values below the level of detection, consisted of 873 paired migration and curvature peaks for the Minnesota River, and 371 peaks for the Root River. There are an additional 873 paired inflections for the Minnesota River, and 585 along the Root River, used to analyze lag

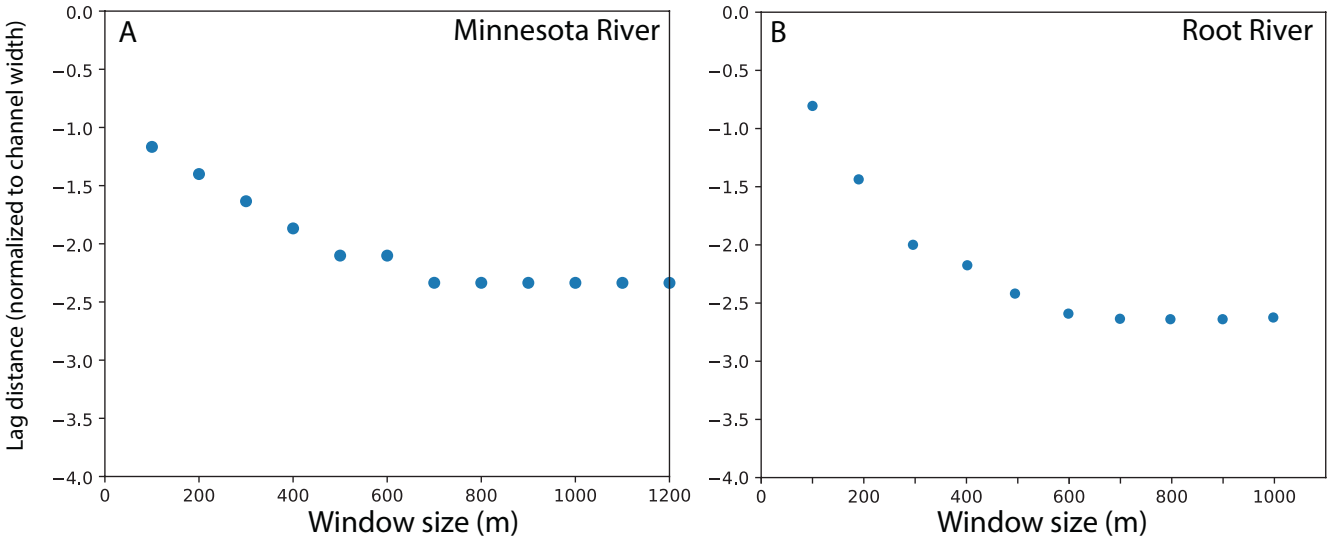

Figure 6. A range of window sizes were tested as input for the cross-correlation analysis. The optimal window size was chosen as the beginning of the sill, which started at 800-m and 600-m search windows for the (a) Minnesota and (b) Root Rivers, respectively. This ensured that the window was wide enough to find the optimal lag but was not excessively large to search beyond relevant signals.

distance between migration and curvature (n_{tot} = 1746). Because cross-correlation analyses do not rely on peaks or inflections, every measurement (excluding cutoffs and measurements below the level of detection) along the study reaches is used, totaling approximately 86,000 and 87,200 points for the Minnesota and Root River study reaches, respectively.

4.2. Optimizing Search Radius of Cross-Correlation Analyses

The cross-correlation analysis identified similar lag distances, scaled to the width of each river, between the curvature and migration rate signals. For the Minnesota River, the optimal window size for analyzing cross-correlations is 800 m, equivalent to 9–12 channel widths (Figure 6a). Similarly, the Root River had an optimal window size of 600 m, ~12× mean channel width (Figure 6b). Outside this range, subsequent increases in window size did not change results and narrower windows were not sufficiently wide to capture the optimized lag distance. These results are illustrated by the consistency in lag distances that begin at 600 m (Figure 6). Thus, windows for the cross-correlation analysis are optimal at lag distances of 800 and 600 m for the Minnesota and Root rivers, respectively. That is, peak cross-correlation coefficients between signals of migration and curvature do not improve beyond window sizes of 9–12 channel widths. Thus, the computation time is minimized by excluding broader window searches while ensuring the optimal lag distance is found. The windows are consistent with lag distances we observed between the curvature and migration signals while manually matching peaks and inflections (e.g., Figure 4).

4.3. Magnitude and Variability of Lags Between Curvature and Migration

The results of 86,000 cross-correlations for the Minnesota River indicate that curvature signals are most significantly correlated with migration rates that are 2.2 (±1.3) channel widths downstream (Figures 7a and 7b). Cross-correlation analysis for the 7,200 points along the Root River was nearly identical with signal offsets of 2.3 (±1.2) (Figures 7c and 7d). All cross-correlation results with low cross-correlation coefficients ($r < 0.25$) were removed from the analysis prior to calculating the mean lag. Such values were irrelevant for discerning an optimal phase lag, which should be based on strong correlation coefficients.

We further analyzed the cross-correlation data along the Minnesota River by separating data for the downstream, low-sediment supply reach (red points, Figure 7a) from the upstream, high-sediment supply reach (blue points). Partitioning the data in this way revealed that only 6% of cross-correlations in the reach with low bedload sediment supply (downstream of Belle Plaine) had strong signal matching (defined as

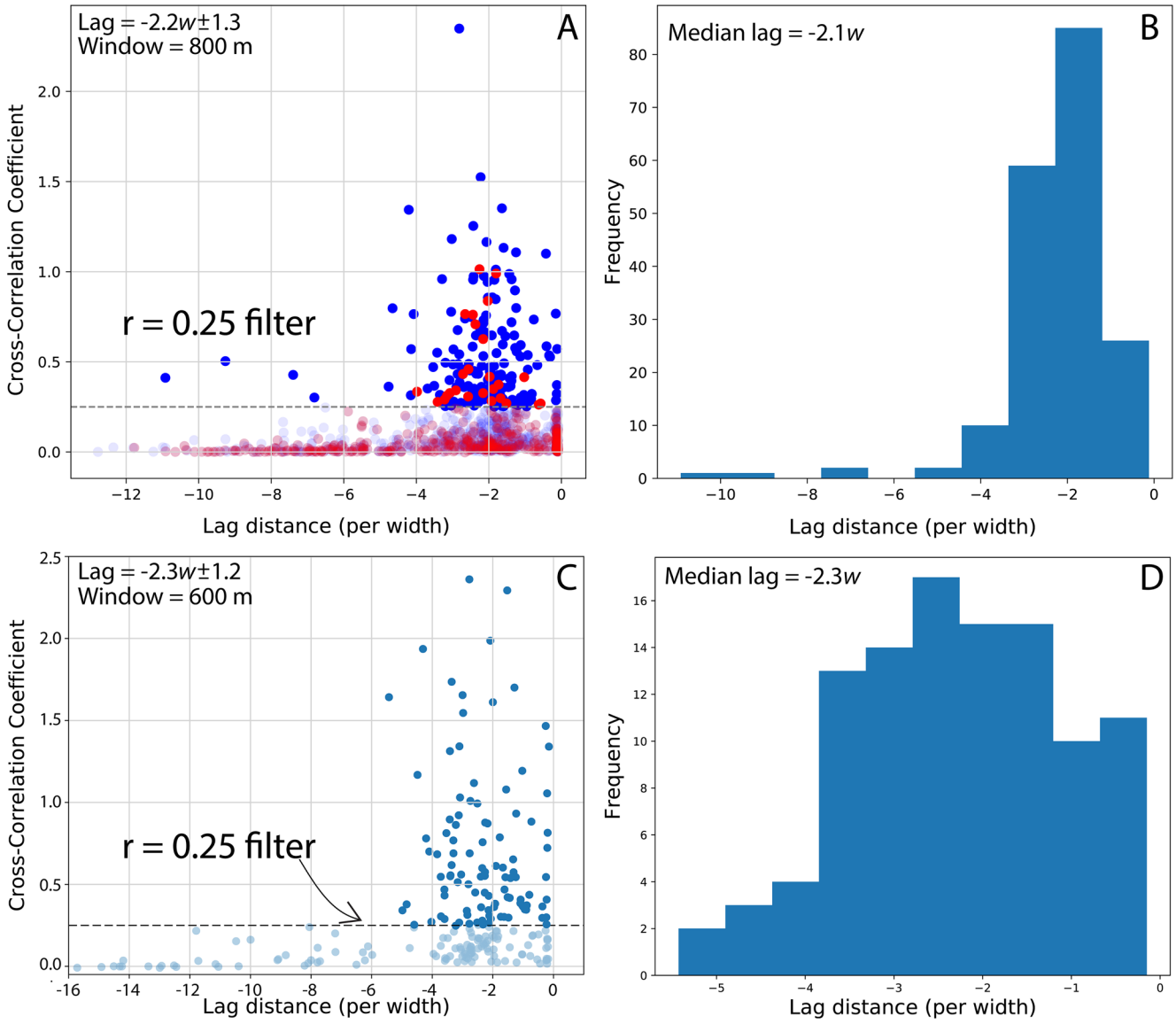

Figure 7. Scatterplot and histogram showing the distribution of lag distances between curvature and migration signals for the Minnesota (a) & (b) and Root (c) & (d) Rivers, based on cross correlation of the curvature and migration rate curves. Similar mean and median lags of −2.2 to −2.3 channel widths for both rivers indicate that the signal of migration is typically a distance of 2.3 channel widths downstream of a correlated signal in curvature (Figures 7b and 7d). We filtered cross-correlations below 0.25 (transparent points) that had weak signal matching and skewed the central tendency. The vast majority (94%) of cross-correlations in the Minnesota River reach with low sediment transport (red-points, 7a) had very low signal matching, indicated by coefficients below 0.25 compared to the upstream reach (blue points, 7a).

$r > 0.25$), compared to reaches with high bedload sediment supply along the upper Minnesota River study reach (30%). The Root River exhibited stronger results yet compared to the Upper Minnesota River study reach, with 50% of the cross-correlations exhibiting high signal matching.

We observed consistent lag distances between curvature and migration rates in our two study rivers. The magnitude and variability for lag distances in peaks (2.5 ± 1.4) and inflections (2.3 ± 1.2) along both reaches of the Minnesota River were remarkably similar to each other (Figures 8a and 8b), and to the phase lags in cross-correlations (2.2 ± 1.3, Figure 7a). The results were also consistent with the lag distances for peaks (2.6 ± 1.4) and inflections (2.8 ± 1.6) along the Root River (Figures 8c and 8d), as well as the cross-correlations between all data (2.3 ± 1.2). The consistency in lag distances for both rivers suggests that peak stress along the outer bank is consistently 2.3–2.8 channel widths downstream of the apex of a meander bend.

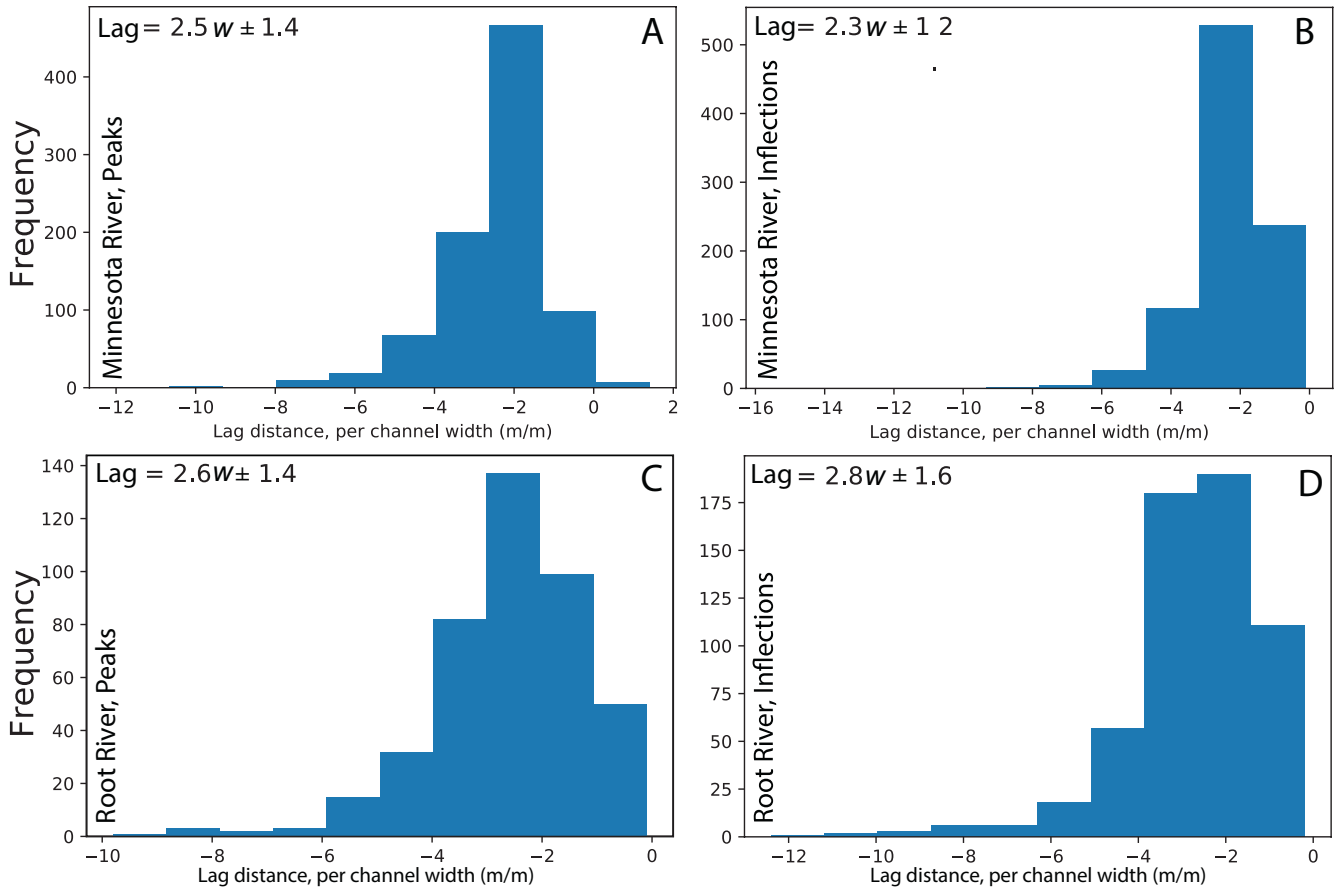

Figure 8. Histograms of lag distances between peaks and inflections (b/d) in curvature and migration for the Minnesota (a & b, top) and Root (c & d, bottom) Rivers. Lag distances (meters) were scaled to channel width for simpler interpretation and comparability with other systems. Similar to results of cross-correlations, lag distances between curvature and migration were typically 2.6X (peaks) to 2.8X (inflections) channel width.

Pairs of curvature-migration peaks were more readily distinguishable in the Minnesota River in the upstream, high bedload reach. Eighty percent (693) of the 873 paired peaks found along the Minnesota River occurred within the upstream, high bedload reach. This strong correlation of peaks can be confirmed qualitatively throughout the upstream high bedload reach (Figure 9a), as profiles of migration rates are very nearly a translated form of the channel curvature trends. In stark contrast, only 20% of paired peaks occurred in the downstream, low bedload reach, which exhibits very little signal similarity between migration rates and channel curvature (Figures 9a and 9b). While we observe similar ranges of curvature in the high and low bedload reaches, the correlation between curvature and migration is completely absent in the low bedload reach (Figure 9b).

4.4. Variables Affecting the Spatial Lag in the Curvature-Migration Relation

We hypothesized that variations in the lag between channel curvature and migration rates would be a function of local curvature or bank erosivity. Local curvature did not have any significant explanatory power in the variance of the measured lag distances. This indicates that the exact lag distance between curvature and migration signals cannot be explained as a function of local curvature alone. A discussion of possible explanatory variables based on theory and observations is provided in subsequent sections. While available data did not allow for quantitative constraints on bank erodibility, our manual categorical classifications along the Root River did not suggest that erodibility increased lag distance. Observations of partially confined reaches suggest that constricted bends exhibit downstream translation that shift migration trajectories downstream of what would be expected from curvature-migration lag distances described above (Inset 1, Figure 10) compared to freely meandering bends (Inset 2).

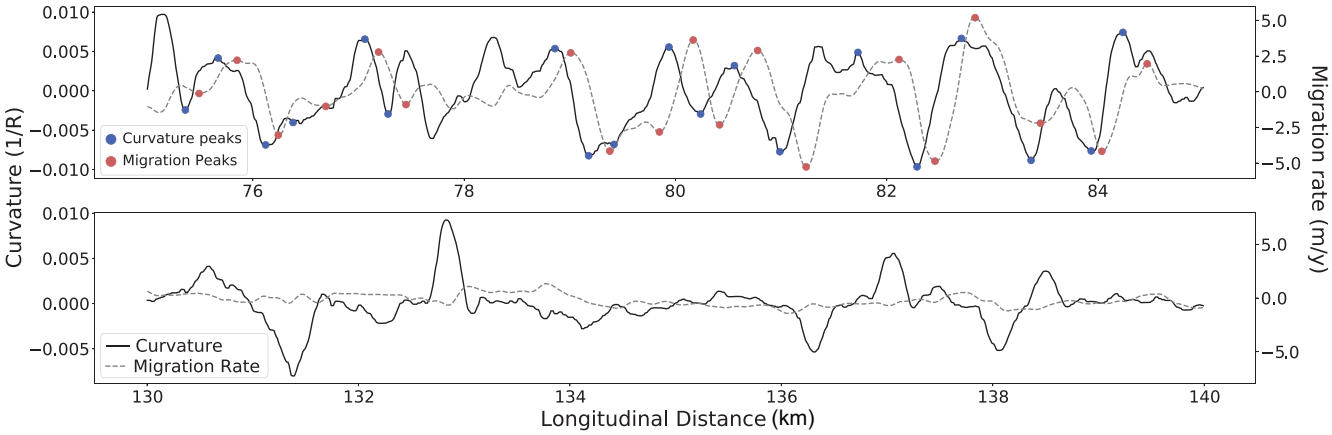

Figure 9. Longitudinal profiles of migration rate (gray-dashed lines) and curvature (solid black lines) for two distinct 10-km reaches of the 180-km Minnesota River study area. The top profile is from the upstream portion of our study reach with steeper slopes and high sediment supply of coarse-grained sediments (sand and gravel). The lower profile is from the downstream reach with lower slopes and sediment supply of fine sand, silt, and clay. (a) Curvature and migration signals show strong spatially lagged signals and have many paired peaks (red and blue points). (b) Despite a similar range of curvature values as the top reach, the migration rates are nearly zero, and lack any resemblance of a lagged signal. The paucity of paired curvature-migration peaks (red and blue points) in the downstream reach demonstrate the influence of sediment supply on lateral channel migration and channel curvature.

4.5. Spatial Scale-Dependence of the Curvature-Migration Relation

To explore the nature of the curvature-migration relationship, we plotted bend-averaged and normalized radius of curvature (R/W) and normalized migration rates (M/W) as found in previous empirical studies (Finotello et al., 2018; Hickin & Nanson, 1984; Hooke, 2003; Hudson & Kesel, 2000; Nicoll & Hickin, 2010). This measurement approach results in an envelope of values that are generally scattered, with some values peaking near R/W of 2–3 (Figures 11a and 11b). Next, we consider the trends that arise when we plot spatially lagged dimensionless curvature and normalized migration rates (Figures 12 and 13). For both the Minnesota and Root Rivers, the relationship between channel curvature and migration rates is generally simple monotonic trends that are fit reasonably well with linear regressions. Thus, differences in measurement scale and taking into account the spatial lag influence the apparent relationship between channel curvature and migration rate.

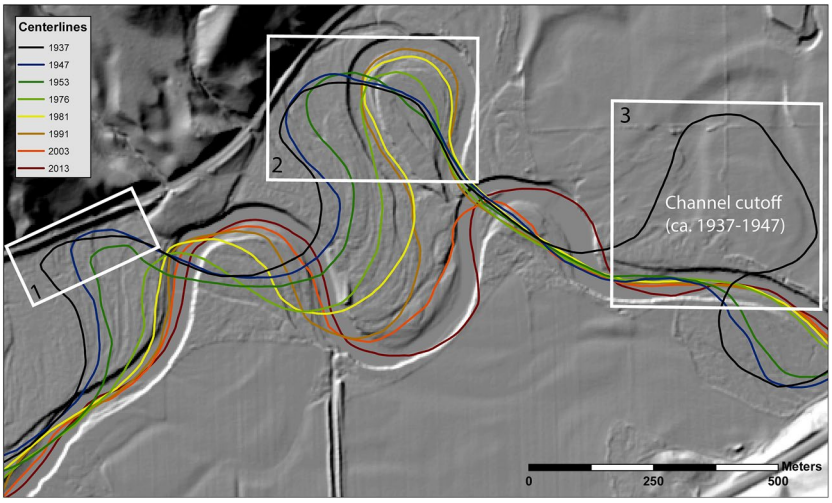

Figure 10. Planform view of channel changes from 1937 to 2013 (black to maroon sequence). Inset areas illustrating: (a) a valley wall constriction is inhibiting river migration directly downstream of the bend apex, resulting in downstream migration; (b) typical downstream shift of peak migration relative to the apex in curvature; (c) example of a channel cutoff that occurred between 1937 (black) and 1947 (blue).

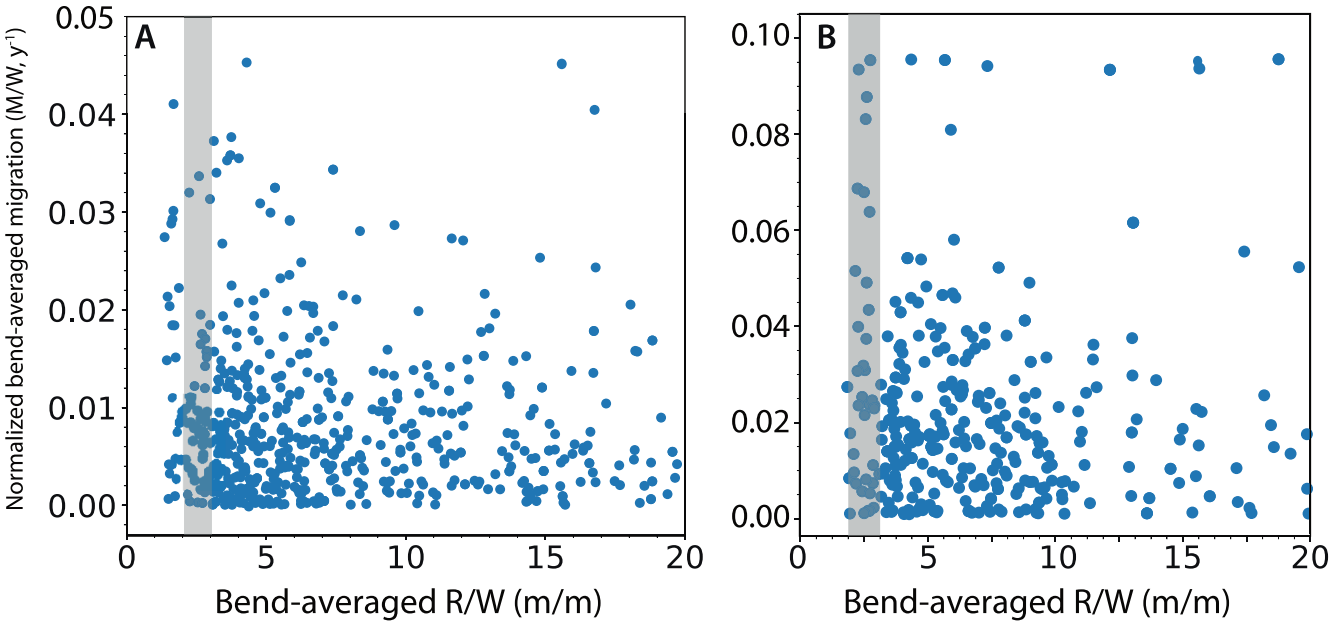

Figure 11. Bend-averaged migration and curvature plotted in accordance with Hickin and Nanson (1975) for the (a) Minnesota River and (b) Root River. Few of the data peak at values near or larger than the range of R/W values (2–3) expected by Hickin & Nanson's envelope curve (gray-shaded region), while others are void of any strong trend. This approach conflates fine-scale changes in curvature by averaging over the entire bend and fails to account for lags between migration and curvature.

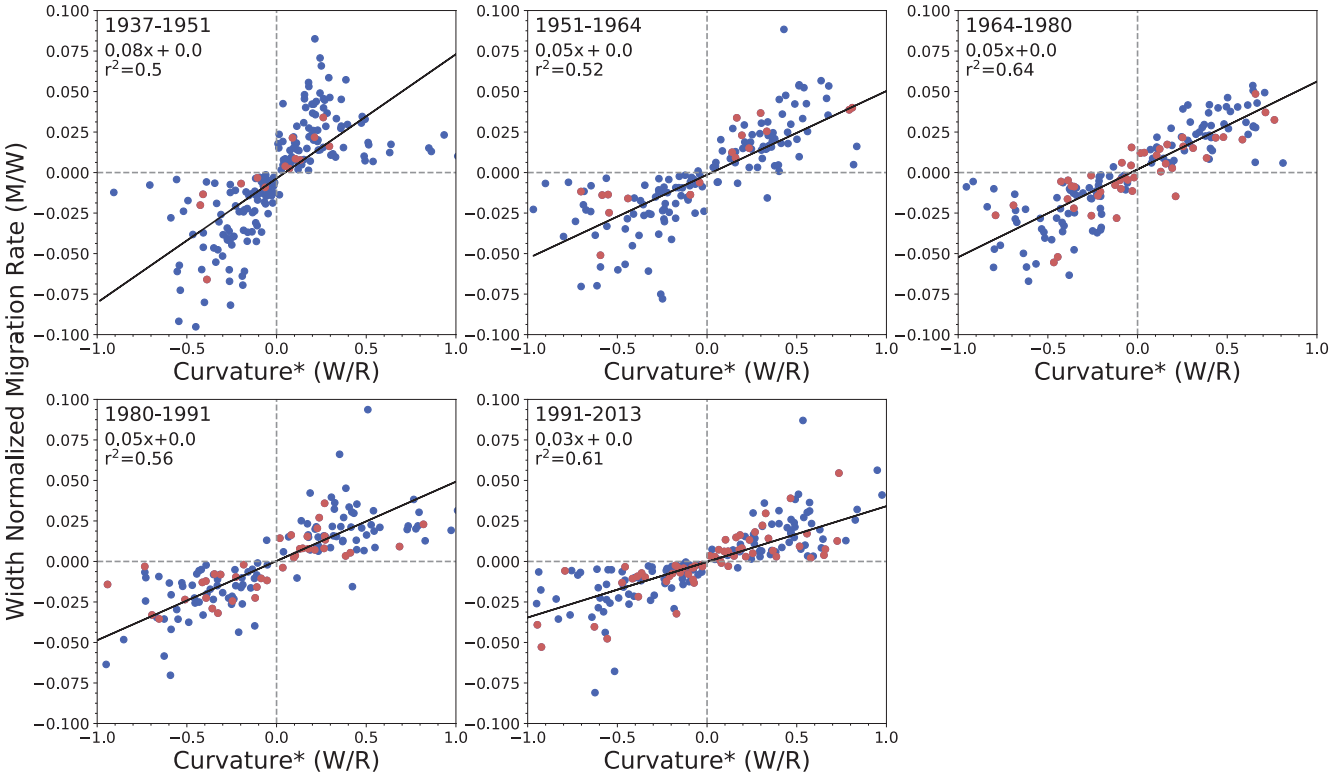

Figure 12. Relationships between dimensionless curvature (W/R) and normalized migration rates (M/W) for the Minnesota River. Most years follow linear trends, with the exception of the first plot. Red data points are for the downstream portion of the study reach where sediment transport rates were significantly lower than the upstream reach (blue points). Regressions include upstream and downstream reaches.

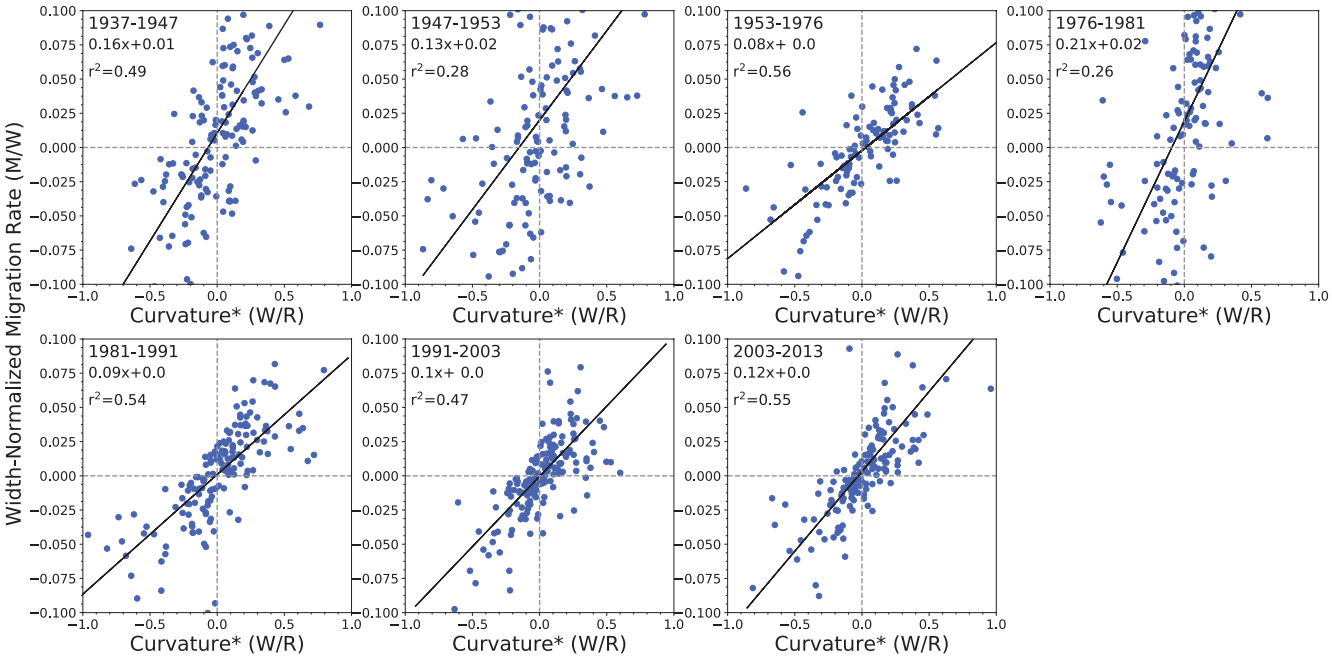

Figure 13. Relationships between dimensionless curvature (W/R) and normalized migration rates (M/W) for the Root River. All years exhibit linear trends, with similar slopes (0.1–0.2) and intercepts near 0.

Within each study site, the relationships exhibit positive slopes with intercepts at or near zero. For the Minnesota River, regression slopes ranged from 0.03 to 0.08 (Figure 12), while regression slopes for Root River were much higher, on the order of 0.1–0.2 (Figure 13). The exact cause of distinctly lower slope regressions for the Minnesota River could not be determined. Notably, regression slopes for the Minnesota River decrease in time toward the present, while the Root River regression slopes are temporally stationary with the exception of 1976–1981.

5. Discussion

Empirical results herein support multiple previous studies indicating that migration rates peak downstream of bend apices (Furbish, 1988; Howard & Knutson, 1984; Seminara, 2006; Sylvester, Durkin, & Covault, 2019). For the Minnesota and Root Rivers, the lag distance between signals of curvature and migration exhibit a relatively narrow range, between 2.3 and 2.8 channel widths (Figures 7 and 8), which fall within the range of 2.1–4.7 channel widths previously found for Amazonian rivers (Sylvester, Durkin, & Covault, 2019). Our results also match experimental flume results indicating peak shear stress along the outer bank occurred 2.5 channel widths downstream of the bend apex (Figures 7–9; Hooke, 1975). The similarity in lag distances for both of our study sites as well as previous literature suggests that the spatial lag is fairly consistent across a wide range of climates and geological settings.

The relationship between curvature and migration appears to break down under conditions where bedload sediment supply is negligible relative to the transport capacity. Specifically, the strength of signal coherence between curvature and migration rates is significantly diminished where sediment transport is negligible (red points, Figures 7a and 9b) (Groten et al., 2016; Kelly, 2019), suggesting the reach is unable to establish marked asymmetry in bed morphology and associated lateral hydraulic flow paths. The drastic reduction in moderate-to-strong signal correlations and rare occurrence of paired peaks in the downstream, low bedload reach, of the Minnesota River suggests that without significant sediment supply for point bar growth, signal similarity is greatly diminished. This inference is further corroborated by results from the Root River, which has been shown to have significant sediment supply from adjacent streambanks (Belmont, Dogwiler, & Kumarasamy, 2016; Belmont, Dogwiler, Czuba et al., 2016; Vaughan et al., 2017). These results hold regardless of whether we use bend-averaged or spatially explicit and lagged measurements. Mechanisms driving

bar-push and migration appear to be muted and rarely exceed bank resisting forces in reaches without sufficient sediment supply to form bars that are large enough to exert a substantial influence on the flow field (Dietrich et al., 1983).

In this study, we use sub-meander measurement scales to shed light on the spatially lagged relationship between curvature and migration. Many previous studies suggest that migration rates peak at intermediate values of meander-bend curvature (Güneralp & Rhoads, 2008; Hickin & Nanson, 1975; Hooke, 2003; Hudson & Kesel, 2000; Nanson & Hickin 1983; Nicoll & Hickin, 2010). However, these results reflect the use of bend-averaged values of curvature and migration, which smooth over variability occurring at sub-meander bend scales. Our findings from two rivers support both empirical and theoretical work illustrating a simple monotonic relationship between curvature and migration (Furbish, 1988; Howard & Knutson, 1984; Schwenk et al., 2015; Sylvester, Durkin, & Covault, 2019). We expect that variability in lag distances is influenced at least in part by differences in vegetation type (e.g., grass, bush/shrub, tree), bank material (e.g., floodplain, terrace, colluvium), channel constrictions (valley impingements, concrete embankments), bar geometry, local and upstream width-to-depth ratios, channel bedforms, and friction factor. Recent re-analysis of data from the Amazon Basin highlights an interesting leveling off of migration rates at high curvatures (Finotello et al., 2019). It is possible that the data collected in our study do not include a sufficient number of high curvature bends to identify such an effect. However, the idea that migration rates would decrease beyond a certain threshold curvature is not supported by the data from the Amazonian rivers (Sylvester, Durkin, Covault, et al., 2019) or by the data from the Minnesota and Root Rivers presented here.

As channel curvature increases, the rate of increase in migration rates for the Root River are 2- to 4-fold higher than that of the Minnesota River based on the trendlines in Figures 12 and 13. This observation could suggest that lateral flow paths and hydraulic conditions driving meander migration may be accentuated, or resisting forces in the banks may be diminished, in the Root River compared to the Minnesota River. Previous research has demonstrated the importance of migration and widening as a dominant source of sediment for the Root River (Belmont, Dogwiler, & Kumarasamy, 2016; Belmont, Dogwiler, Czuba et al., 2016; Stout et al., 2014) and Vaughan et al. (2017) showed that the Root River has some of the steepest relationships between Q and TSS (discharge-total suspended sediment) in the state of Minnesota, due largely to near-channel sediment sources. So, while we do not have bedload data for the Root River, there is good reason to believe that sediment transport rates are high in that system, similar to the upstream reach of the Minnesota River and in contrast to the downstream reach of the Minnesota River.

6. Conclusions & Future Research

Our results from both the Minnesota and Root Rivers indicate that the relationship between curvature and migration rate breaks down in reaches with low bedload sediment supply (Figures 7a and 9b). Migration rates are slow and signal coherence between curvature and migration is low in the downstream, low bedload reach of the Minnesota River, compared with the upstream reach of the Minnesota River and the Root River, both of which have high rates of bedload sediment transport. The mechanistic linkage between bedload sediment transport and the curvature-migration relationship, we propose, is related to the influence of bars on the hydraulics of curved channels. Specifically, higher bedload transport, relative to transport capacity, increases the size and width of bars and therefore accentuates the lateral and helical flow patterns in curved channels. As a result, the spatially lagged relationship between channel curvature and migration rate is stronger.

The knowledge gleaned herein from studying feedbacks between channel curvature and sediment supply demonstrate how each plays an important role in meander migration. The spatially lagged relationship in which curvature matches signals of migration rates by 2.3–2.8 channel widths downstream appears consistent across multiple settings, including laboratory flume as well as natural rivers in distinct lithologies and climates as long as bedload sediment transport is relatively high (i.e., Hooke, 1975; Sylvester, Durkin, & Covault, 2019; this study). Additional field, experimental and numerical modeling research is needed to develop a more complete, predictive understanding of how bedload transport, supply and depositional processes influence bar morphology and flow field dynamics and ultimately modulate the curvature-migration rate relation. While aerial imagery has been sufficient to highlight the differences between reaches with

and without ample sediment supply, incorporating three-dimensional bed topography and bed-sediment sampling would enable a more robust understanding of such complex interactions. In order to make mechanistic inferences and associations between these variables, measurement scales must be sufficiently fine to resolve sub-meander scale variability in underlying physical mechanisms such as shear stress (Dietrich et al., 1979; Hooke, 1975; Seminara, 2006).

Our results from the Minnesota and Root Rivers also highlight the importance of measurement length scales in interpretation of form-process relations. In previous studies investigating the relation between channel curvature and lateral channel migration rates, measurements averaged over the scale of a reach or single meander bend provide useful insights when driving mechanisms do not vary significantly over such scales. However, issues arise when spatial averaging obscures the spatial heterogeneity occurring at finer scales, which diminishes the opportunity to make accurate inferences of mechanisms driving migration rates. Plots comparing bend-averaged radius of curvature with migration rates contain two common features: (1) multiple migration rates can be associated with a single curvature value, and (2) migration rates appear to fall at low radius of curvature values (e.g., Hickin & Nanson, 1984; Hooke, 1987; Hudson & Kesel, 2000). The former arises because bend-averaged curvature smooths over variability in shear stress throughout a meander bend (Furbish, 1988, 1991). The latter is the result of comparing local channel curvature and migration rate measurements and is the result of the downstream shift of maximum migration rate relative to the bend apex (Sylvester, Durkin, & Covault, 2019).

Understanding the relationship between channel curvature and migration rate is improved when using measurement length scales that resolve the variability in shear stress along meander bends. Analyses should compare channel curvature values with migration rates ~2–3 channel widths downstream; the average lag distance can be estimated by cross-correlating the curvature and migration rate series. Additional research is needed to better understand factors influencing variation in lag distance.

Data Availability Statement

Centerline shapefiles, migration calculations, and all python scripts used herein have been made available at: https://usu.box.com/s/8x197r3ivv1kr3n53mqbtn1tpm7tbr16. For imagery and base layers used for delineations, access can be found through the Minnesota Geospatial Information Office, here: http://www.mngeo.state.mn.us/chouse/wms/wms_image_server_layers.html.

Acknowledgments
In addition to our funding, the authors thank Peter Wilcock, Sara Null, and Chris Garrard for input and feedback for the methods and algorithms along the way. Additional ideas and assistance with bank digitization were provided by Bastiaan Notebaert, Shannon Belmont, Devon Libby, Adam Fisher. The authors extend additional thanks to Amy East, Noah Finnegan, and three anonymous reviewers for their extensive feedback that improved the work found herein. This work was supported by the Quinney Foundation, National Science Foundation (NSF ENG 1209445), Minnesota Department of Agriculture, and Utah State University. The work also received support from the Utah Agricultural Experiment Station.

References

Abernethy, B., & Rutherfurd, I. D. (2000). The effect of riparian tree roots on the mass-stability of riverbanks. *Earth Surface Processes and Landforms*, *25*, 921–937. https://doi.org/10.1002/1096-9837(200008)25:9<921::AID-ESP93>3.0.CO;2-7

Ashworth, P. J. (1996). Mid-channel bar growth and its relationship to local flow strength and direction. *Earth Surface Processes and Landforms*, *21*(2), 103–123. https://doi.org/10.1002/(SICI)1096-9837(199602)21:2<103::AID-ESP569>3.0.CO;2-O

Bagnold, R. A. (1960). *Some aspects of river meanders professional paper 282-E*. United States Geological Survey.

Begin, Z. B. (1981). Stream curvature and bank erosion: A model based on the momentum equation. *The Journal of Geology*, *89*, 497–504. https://doi.org/10.1086/628610

Belmont, P. (2011). Floodplain width adjustments in response to rapid base level fall and knickpoint migration. *Geomorphology*, *128*, 92–102. https://doi.org/10.1016/j.geomorph.2010.12.026

Belmont, P., Dogwiler, T., & Kumarasamy, K. (2016). *An integrated sediment budget for the Root river watershed, Southeastern Minnesota*. Final Report to the Minnesota Department of Agriculture. Minnesota Department of Agriculture.

Belmont, P., Gran, K. B., Schottler, S. P., Wilcock, P. R., Day, S. S., Jennings, C., et al. (2011). Large shift in source of fine sediment in the upper Mississippi river. *Environmental Science & Technology*, *45*, 8804–8810. https://doi.org/10.1021/es2019109

Belmont, P., Stevens, J. R., Czuba, J. A., Kumarasamy, K., & Kelly, S. A. (2016). Comment on "Climate and agricultural land use change impacts on streamflow in the upper midwestern United States" by Gupta et al. *Water Resources Research*, *52*(9), 7523–7528.

Blanckaert, K. (2011). Hydrodynamic processes in sharp meander bends and their morphological implications. *Journal of Geophysical Research: Earth Surface*, *116*(F1). https://doi.org/10.1029/2010JF001806

Brice, J. C. (1974). Evolution of meander loops. *GSA Bulletin*, *85*, 581–586. https://doi.org/10.1130/0016-7606(1974)85<581:EOML>2.0.CO;2

Call, B. C., Belmont, P., Schmidt, J. C., & Wilcock, P. R. (2017). Changes in floodplain inundation under nonstationary hydrology for an adjustable, alluvial river channel. *Water Resources Research*, *53*(5), 3811–3834.

Carson, M. A., & Lapointe, M. F. (1983). The inherent asymmetry of river meander planform. *The Journal of Geology*, *91*, 41–55. https://doi.org/10.1086/628743. https://doi.org/10.1002/2016WR020277

Clayton, L., & Moran, S. R. (1982). Chronology of late Wisconsinan glaciation in middle North America. *Quaternary Science Reviews*, *1*, 55–82. https://doi.org/10.1016/0277-3791(82)90019-1

Constantine, J. A., Dunne, T., Ahmed, J., Legleiter, C., & Lazarus, E. D. (2014). Sediment supply as a driver of river meandering and floodplain evolution in the Amazon Basin. *Nature Geoscience*, *7*, 899–903. https://doi.org/10.1038/ngeo2282

Davis, W. M. (1902). *River terraces in New England*. In Geographical essays (pp. 514–586). Ginn and Co.

Dietrich, W. E., & Smith, J. D. (1983). Influence of the point bar on flow through curved channels. *Water Resources Research*, *19*(5), 1173–1192.
Dietrich, W. E., Smith, J. D., & Dunne, T. (1979). Flow and sediment transport in a sand bedded meander. *The Journal of Geology*, *87*, 305–315. https://doi.org/10.1086/628419
Donovan, M., & Belmont, P. (2019). Timescale dependence in river channel migration measurements. *Earth Surface Processes and Landforms*, *44*(8), 1530–1541. https://doi.org/10.1002/esp.4590
Donovan, M., Miller, A., & Baker, M. (2016). Reassessing the role of milldams in Piedmont floodplain development and remobilization. *Geomorphology*, *268*, 133–145. https://doi.org/10.1016/j.geomorph.2016.06.007
Donovan, M., Miller, A., Baker, M., & Gellis, A. (2015). Sediment contributions from floodplains and legacy sediments to Piedmont streams of Baltimore county, Maryland. *Geomorphology*, *235*, 88–105. https://doi.org/10.1016/j.geomorph.2015.01.025
Einstein, A. (1926). Die Ursache der Mäanderbildung der Flußläufe und des sogenannten Baerschen Gesetzes—"The cause of the formation of meanders in the courses of rivers and of the so called Baer's law. *Die Naturwissenschaften*, *14*, 223–224. https://doi.org/10.1007/BF01510300
Eke, E., Parker, G., & Shimizu, Y. (2014). Numerical modeling of erosional and depositional bank processes in migrating river bends with self-formed width: Morphodynamics of bar push and bank pull: Modeling bank processes in river bends. *Journal of Geophysical Research: Earth Surface*, *119*(7), 1455–1483. https://doi.org/10.1002/2013JF003020
Ellis, D. (2014). *dp_python, optimized dynamic programming (DP)/dynamic time warp (DTW) as a Python external*. New York City: Dan Ellis. Retrieved from https://github.com/dpwe/dp_python
Engel, F. L., & Rhoads, B. L. (2012). Interaction among mean flow, turbulence, bed morphology, bank failures and channel planform in an evolving compound meander loop. *Geomorphology*, *163–164*, 70–83. https://doi.org/10.1016/j.geomorph.2011.05.026
Finotello, A., D'Alpaos, A., Lazarus, E. D., & Lanzoni, S. (2019). Comment on: High curvatures drive river meandering. *Geology*, *47*(10), e485. https://doi.org/10.1130/G46761C.1
Finotello, A., Lanzoni, S., Ghinassi, M., Marani, M., Rinaldo, A., & D'Alpaos, A. (2018). Field migration rates of tidal meanders recapitulate fluvial morphodynamics. *Proceedings of the National Academy of Sciences*, *115*(7), 1463–1468. https://doi.org/10.1073/pnas.1711330115
Foufoula-Georgiou, E., Takbiri, Z., Czuba, J. A., & Schwenk, J. (2015). The change of nature and the nature of change in agricultural landscapes: Hydrologic regime shifts modulate ecological transitions. *Water Resources Research*, *51*(8), 6649–6671. https://doi.org/10.1002/2015WR017637
Furbish, D. J. (1988). River-bend curvature and migration: How are they related? *Geology*, *16*, 752–755. https://doi.org/10.1130/0091-7613(1988)016<0752:RBCAMH>2.3.CO;2
Furbish, D. J. (1991). Spatial autoregressive structure in meander evolution. *GSA Bulletin*, *103*, 1576–1589. https://doi.org/10.1130/0016-7606(1991)103<1576:SASIME>2.3.CO;2
Gaeuman, D., Symanzik, J., & Schmidt, J. C. (2005). A map overlay error model based on boundary geometry. *Geographical Analysis*, *37*, 350–369. https://doi.org/10.1111/j.1538-4632.2005.00585.x
Gran, K. B., Finnegan, N., Johnson, A. L., Belmont, P., Wittkop, C., & Rittenour, T. (2013). Landscape evolution, valley excavation, and terrace development following abrupt postglacial base-level fall. *Geological Society of America Bulletin*, *125*, 1851–1864. https://doi.org/10.1130/B30772.1
Groten, J. T., Ellison, C. A., & Hendrickson, J. L. (2016). Suspended-sediment concentrations, bedload, particle sizes, surrogate measurements, and annual sediment loads for selected sites in the lower Minnesota river basin, water years 2011 through 2016 (Scientific investigations Report No. 2016-5174). Department of Interior, U.S. Geological Survey.
Güneralp, İ., & Marston, R. A. (2012). Process–form linkages in meander morphodynamics: Bridging theoretical modeling and real world complexity. *Progress in Physical Geography: Earth and Environment*, *36*, 718–746. https://doi.org/10.1177/0309133312451989
Güneralp, İ., & Rhoads, B. L. (2008). Continuous characterization of the planform geometry and curvature of meandering rivers: Planform geometry and curvature of meandering rivers. *Geographical Analysis*, *40*, 1–25. https://doi.org/10.1111/j.0016-7363.2007.00711.x
Güneralp, İ., & Rhoads, B. L. (2009). Empirical analysis of the planform curvature-migration relation of meandering rivers. *Water Resources Research*, *45*. https://doi.org/10.1029/2008WR007533
Güneralp, İ., Rhoads, B. L., (2011). Influence of floodplain erosional heterogeneity on planform complexity of meandering rivers. *Geophysical Research Letters*, *38*. https://doi.org/10.1029/2011GL048134
Gurnell, A. M., Downward, S. R., & Jones, R. (1994). Channel planform change on the river Dee Meanders, 1876–1992. *Regulated Rivers: Research & Management*, *9*, 187–204. https://doi.org/10.1002/rrr.3450090402
Hickin, E., & Nanson, G. (1984). Lateral migration rates of river bends. *Journal of Hydraulic Engineering*, *110*, 1557–1567. https://doi.org/10.1061/(ASCE)0733-9429(1984)110:11(1557)
Hickin, E. J., & Nanson, G. C. (1975). The character of channel migration on the Beatton river, northeast British Columbia, Canada. *GSA Bulletin*, *86*, 487–494. https://doi.org/10.1130/0016-7606(1975)86<487:TCOCMO>2.0.CO;2
Hooke, J. M. (1987). Changes in meander morphology. In V. Gardiner (Ed.), *Proceedings of the First International Conference on Geomorphology*, (Vol. 1, pp. 591–609). Chinchester, U.K.: Wiley.
Hooke, J. (2003). River meander behavior and instability: A framework for analysis: River meander behavior and instability. *Transactions of the Institute of British Geographers*, *28*, 238–253. https://doi.org/10.1111/1475-5661.00089
Hooke, R. L. B. (1975). Distribution of sediment transport and shear stress in a meander bend. *The Journal of Geology*, *83*, 543–565. https://doi.org/10.1086/628140
Howard, A. (1996). Modeling channel evolution and floodplain morphology. In *Floodplain processes* (pp. 15–62). John Wiley & Sons.
Howard, A. D., & Knutson, T. R. (1984). Sufficient conditions for river meandering: A simulation approach. *Water Resources Research*, *20*, 1659–1667. https://doi.org/10.1029/WR020i011p01659
Hudson, P. F., & Kesel, R. H. (2000). Channel migration and meander-bend curvature in the lower Mississippi River prior to major human modification. *Geology*, *28*, 531–534. https://doi.org/10.1130/0091-7613(2000)28<531:CMAMCI>2.0.CO;2
Jennings, C. E. (2010). Draft digital Reconnaissance surficial geology and geomorphology of the Le Sueur river watershed (blue Earth, Waseca, Faribault, and freeborn counties in south-central MN) (No. Open file Report 10-03), map, Report, and digital files. Minnesota Geological Survey.
Kasvi, E., Laamanen, L., Lotsari, E., & Alho, P. (2017). Flow patterns and morphological changes in a Sandy Meander bend during a flood—Spatially and temporally intensive ADCP measurement approach. *Water*, *9*, 106. https://doi.org/10.3390/w9020106
Kelly, S. A., Takbiri, Z., Belmont, P., & Foufoula-Georgiou, E. (2017). Human amplified changes in precipitation-runoff patterns in large river basins of the Midwestern United States. *Hydrology and Earth System Sciences Discussions*, 1–37. https://doi.org/10.5194/hess-2017-133

Kelly, S., & Belmont, P. (2018). High resolution monitoring of river bluff erosion reveals failure mechanisms and geomorphically effective flows. *Water*, *10*, 394. https://doi.org/10.3390/w10040394

Kelly, S. A. (2019). River hydrology, morphology, and Dynamics in an intensively managed, transient Landscape (doctoral dissertation). Utah State University.

Lauer, J. W., Echterling, C., Lenhart, C., Belmont, P., & Rausch, R. (2017). Air-photo based change in channel width in the Minnesota River basin: Modes of adjustment and implications for sediment budget. *Geomorphology*, *297*, 170–184. https://doi.org/10.1016/j.geomorph.2017.09.005

Lauer, J. W., & Parker, G. (2008). Net local removal of floodplain sediment by river meander migration. *Geomorphology*, *96*, 123–149. https://doi.org/10.1016/j.geomorph.2007.08.003

Lenhart, C. F., Titov, M. L., Ulrich, J. S., Nieber, J. L., & Suppes, B. J. (2013). The role of hydrologic alteration and riparian vegetation dynamics in channel evolution along the lower Minnesota river. *Transactions of the American Society of Agricultural and Biological Engineers, Erosion and Landscape Evolution*, *56*, 549–561.

Leopold, L. B., & Wolman, M. G. (1960). River Meanders. *GSA Bulletin*, *71*, 769–793. https://doi.org/10.1130/0016-7606(1960)71[769:RM\2.0.CO;2

Lepper, K., Fisher, T. G., Hajdas, I., & Lowell, T. V. (2007). Ages for the Big Stone Moraine and the oldest beaches of glacial Lake Agassiz: Implications for deglaciation chronology. *Geology*, *35*, 667. https://doi.org/10.1130/G23665A.1

Libby, D. J. (2017). Assessing historical planform channel change in an altered watershed with quantification of error and uncertainty present in a GIS/aerial photography-based analysis; case study: Minnesota river, Minnesota, USA (thesis). Minnesota State University.

Lisiecki, L. E., & Lisiecki, P. A. (2002). Application of dynamic programming to the correlation of paleoclimate records: Dynamic programming signal correlation. *Paleoceanography*, *17*, 1–12. https://doi.org/10.1029/2001PA000733

Martinelli, L. A., Victoria, R. L., Devol, A. H., Richey, J. E., & Forsberg, B. R. (1989). Suspended sediment load in the Amazon basin: An overview. *GeoJournal*, *19*. https://doi.org/10.1007/BF00176907

Matsch, C. L. (1983). River Warren, the southern outlet of Lake Agassiz. In J. T. Teller, & L. Clayton (Eds.), *Glacial Lake Agassiz, special paper* (pp. 232–244). Geological Society of Canada.

Micheli, E. R., & Kirchner, J. W. (2002). Effects of wet meadow riparian vegetation on streambank erosion. 1. Remote sensing measurements of streambank migration and erodibility. *Earth Surface Processes and Landforms*, *27*, 627–639. https://doi.org/10.1002/esp.338

Milliman, J. D., & Meade, R. H. (1983). World-wide delivery of river sediment to the oceans. *The Journal of Geology*, *91*, 1–21. https://doi.org/10.1086/628741

Minnesota Department of Natural Resources and Minnesota Geospatial Information Office. (2012). *Hillshade, Lidar-derived, Minnesota*. Minnesota Department of Natural Resources and Minnesota Geospatial Information Office. Retrieved from https://resources.gisdata.mn.gov/pub/gdrs/data/pub/us_mn_state_mngeo/elev_lidar_hillshade/metadata/metadata.html

Morais, E. S., Rocha, P. C., & Hooke, J. (2016). Spatiotemporal variations in channel changes caused by cumulative factors in a meandering river: The lower Peixe river, Brazil. *Geomorphology*, *273*, 348–360. https://doi.org/10.1016/j.geomorph.2016.07.026

Motta, D., Abad, J. D., Langendoen, E. J., & Garcia, M. H. (2012). A simplified 2D model for meander migration with physically-based bank evolution. *Geomorphology*, *163*, 10–25. https://doi.org/10.1016/j.geomorph.2011.06.036

Nanson, G. C., & Hickin, E. J. (1983). Channel Migration and Incision on the Beatton River. *Journal of Hydraulic Engineering*, *109*(3), 327–337. https://doi.org/10.1061/(ASCE)0733-9429(1983)109:3(327)

Neill, C. R. (1971). River bed transport related to meander migration rates. *Journal of the Waterways, Harbors and Coastal Engineering Division*, *97*(4), 783–786.

Neill, C. R. (1984). *Inter-action of bank erosion and bed-load transport in a shifting gravel river*. In river meandering (pp. 204–211). American Society of Civil Engineers.

Nicoll, T. J., & Hickin, E. J. (2010). Planform geometry and channel migration of confined meandering rivers on the Canadian prairies. *Geomorphology*, *116*, 37–47. https://doi.org/10.1016/j.geomorph.2009.10.005

Novotny, E. V., & Stefan, H. G. (2007). Stream flow in Minnesota: Indicator of climate change. *Journal of Hydrology*, *334*(3–4), 319–333. https://doi.org/10.1016/j.jhydrol.2006.10.011

Patnaik, M., Patra, K. C., Khatua, K. K., & Mohanty, L. (2014). Modeling boundary shear stress in highly sinuous meandering channels. *ISH Journal of Hydraulic Engineering*, *20*, 161–168. https://doi.org/10.1080/09715010.2013.860733

Peixoto, J. M. A., Nelson, B. W., & Wittmann, F. (2009). Spatial and temporal dynamics of river channel migration and vegetation in central Amazonian white-water floodplains by remote-sensing techniques. *Remote Sensing of Environment*, *113*, 2258–2266. https://doi.org/10.1016/j.rse.2009.06.015

Savitzky, A., & Golay, M. J. E. (1964). Smoothing and differentiation of data by simplified least squares procedures. *Analytical Chemistry*, *36*, 1627–1639. https://doi.org/10.1021/ac60214a047

Schwenk, J., Lanzoni, S., & Foufoula-Georgiou, E. (2015). The life of a meander bend: Connecting shape and dynamics via analysis of a numerical model. *Journal of Geophysical Research: Earth Surface*, *120*(4), 690–710. https://doi.org/10.1002/2014JF003252

Schottler, S. P., Ulrich, J., Belmont, P., Moore, R., Lauer, J. W., Engstrom, D. R., & Almendinger, J. E. (2014). Twentieth century agricultural drainage creates more erosive rivers. *Hydrological Processes*, *28*, 1951–1961. https://doi.org/10.1002/hyp.9738

Schumm, S. A. (1965). Patterns of alluvial rivers. *Annual Review of Earth and Planetary Sciences*, *13*, 5–27.

Seminara, G. (2006). Meanders. *Journal of Fluid Mechanics*, *554*, 271. https://doi.org/10.1017/S0022112006008925

Shay, C. T. (1967). *Vegetation history of the southern Lake Agassiz basin during the past 12,000 years*. In Life, land, and water: Paper presented at Proceedings of the 1960 conference on environmental studies of the Glacial Lake Agassiz basin (pp. 231–252). University of Manitoba Press.

Souffront, M. (2014). Channel adjustment and channel-floodplain sediment exchange in the Root river, Southeastern Minnesota (M.S. Thesis). Utah State University.

Stout, J. C., & Belmont, P. (2013). TerEx Toolbox for semi-automated selection of fluvial terrace and floodplain features from lidar. *Earth Surface Processes and Landforms*, *39*, 569–580. https://doi.org/10.1002/esp.3464

Stout, J. C., Belmont, P., Schottler, S. P., & Willenbring, J. K. (2014). Identifying sediment sources and sinks in the root river, southeastern Minnesota. *Annals of the Association of American Geographers*, *104*, 20–39. https://doi.org/10.1080/00045608.2013.843434

Sun, T., Meakin, P., Jøssang, T., & Schwarz, K. (1996). A Simulation Model for Meandering Rivers. *Water Resources Research*, *32*, 2937–2954. https://doi.org/10.1029/96WR00998

Sylvester, Z., Durkin, P., & Covault, J. A. (2019). High curvatures drive river meandering. *Geology*, *47*, 263–266. https://doi.org/10.1130/G45608.1

Sylvester, Z., Durkin, P., Covault, J. A., & Sharman, G. R. (2019). High curvatures drive river meandering: REPLY. *Geology*, *47*(10), e486. https://doi.org/10.1130/G46838Y.1

Vaughan, A. A., Belmont, P., Hawkins, C. P., & Wilcock, P. (2017). Near-channel versus watershed controls on sediment rating curves: Controls on sediment rating curves. *Journal of Geophysical Research: Earth Surface*, *122*(10), 1901–1923. https://doi.org/10.1002/2016JF004180

Venditti, J. G., Nelson, P. A., Minear, J. T., Wooster, J., & Dietrich, W. E. (2012). Alternate bar response to sediment supply termination. *Journal of Geophysical Research*, *117*(F2). https://doi.org/10.1029/2011JF002254

Wolman, M. G., & Leopold, L. B. (1957). *River flood plains: Some observations on their formation (USGS professional paper No. 282-C)*. U.S. Geological Survey-US Government Printing Office.

Zhou, J., Chang, H. H., & Stow, D. (1993). A model for phase lag of secondary flow in river meanders. *Journal of Hydrology*, *146*, 73–88. https://doi.org/10.1016/0022-1694(93)90270-J